Theor Chem Acc (1997) 98:155–164

Theoretical
Chemistry Accounts

Regular Article

FSGO band structure calculations of polyethers in Fourier space

I. Flamant[1], **J.G. Fripiat**[2], **J. Delhalle**[1]

[1] Laboratoire de Chimie Théorique des Surfaces et des Interfaces, Facultés Universitaires Notre-Dame de la Paix, Rue de Bruxelles 61, B-5000 Namur, Belgium
[2] Laboratoire de Chimie Théorique Appliquée, Facultés Universitaires Notre-Dame de la Paix, Rue de Bruxelles 61, B-5000 Namur, Belgium

Received: 10 July 1997 / Accepted: 20 August 1997

Abstract. The performance of floating spherical Gaussian orbital basis sets in the description of specific but subtle cooperative interactions such as those occurring between hydrogen atoms (hyperconjugation) or between lone pairs is discussed. The calculations on infinite chains are performed using a Fourier representation of the restricted Hartree-Fock equations. The principle advantage of the method is to ensure that the lattice summations appearing in the Coulomb and exchange terms are carried out accurately and efficiently.

Key words: Restricted Hartree-Fock – Fourier space – Floating spherical Gaussian orbital – Polymers – Band structure

1 Introduction

Over the last few years, theoretical and experimental studies have led progressively to an improved understanding of the relationships between electronic and molecular structures of molecular and polymeric systems. Comparisons between quantum mechanical simulated and measured XPS valence-band spectra of oligomers and polymers have shown that the valence part of X-ray photoelectron spectra contains useful information on their primary and secondary structures [1–3]. Theoretical calculations can be used to detect conformational signatures in the measured valence-band spectra and to identify the electronic descriptors relaying the information in the molecular structure. Recently, it has been shown that long-range methylenic hyperconjugation interactions play an important role in conformational signatures and have been identified in the photoemission spectra of polyethylene (PE) films [4, 5] and self-assembled molecular films [6–8].

The approach based on the use of floating spherical Gaussian orbitals (FSGOs), as originally proposed by Frost [9–11] in the mid 1960s and generalized later by Christoffersen et al. [12–14], has also been proposed as an appropriate and practical method for the rapid calculation of electronic properties of polymers [15–18]. The aim of the present work is to investigate the performance of FSGO basis sets in the description of specific cooperative interactions such as those occurring between hydrogen atoms or between lone pairs.

In this study, the FSGO band structure calculations are performed using a Fourier representation of the restricted Hartree-Fock (RHF) equations [19, 20]. Our Fourier transform code (FTCHAIN) is still in the prototype phase and, at the current stage of development, only *s*-type Gaussian atomic orbitals can be considered. Nevertheless, it has already illustrated successfully the merits of the Fourier representation in the context of calculations of the electronic structure of extended chains [21, 22]. Although the aim of this work is to assess the performance of the FSGO model in dealing with questions mentioned at the beginning, the present results also constitute an opportunity to test the FTCHAIN program.

In order to study the potential of FSGOs in the description of long-range hyperconjugation interactions, the FSGO band structures are compared with those obtained within the conventional RHF direct space (DS) approach [23, 24] using the standard minimal STO-3G basis set [25]. The comparison of the FSGO basis to the minimal STO-3G basis is the most appropriate one.

Band calculations are performed on polyoxymethylene (POM) with the unit cell —CH_2—O—, the simplest polymer related to polyethers, and for which a few analyses of conformational influences on the XPS spectral features have been reported [26–29]. This polymer, in which there is an oxygen atom between each methylene group (CH_2), is isoelectronic to PE. This allows comparison of the results reported here to those of the numerous studies on conformational signatures in the valence band of PE [4, 5, 30].

The paper is planned as follows. In the theoretical section, the basic RHF equations which are used and some computational aspects are introduced. Also briefly described in this section are the model systems. In Sect. 3, we assess qualitatively the performance of FSGO basis sets in the description of long-range inter-

Correspondence to: I. Flamant

actions in PE and POM. The paper ends with a few concluding remarks.

2 Theoretical considerations

2.1 Relevant RHF expressions

The RHF-Bloch states $\phi_n(k,\mathbf{r})$ are doubly occupied up to the Fermi energy E_F and orthonormalized as shown in the following equation

$$\int d\mathbf{r}\phi^*_{n'}(k',\mathbf{r})\phi_n(k,\mathbf{r}) = N\delta_{k'k}\delta_{n'n} \ . \tag{1}$$

$N(N\to\infty)$ is the total number of cells in the system, the lattice sites are identified by the integers m, m' and $m''(=0,\pm1,\pm2,\cdots)$, and n and n' are the band indices. In our notation, the wave number k is expressed in units of $2\pi/a_0$ and is defined in the Brillouin zone (BZ), i.e. $k\in\left[-\frac{1}{2},\frac{1}{2}\right]$. The Bloch states

$$\phi_n(k,\mathbf{r}) = \sum_p C_{pn}(k)b_p(k,\mathbf{r}) \tag{2}$$

are expressed in terms of Bloch sums $b_p(k,\mathbf{r})$,

$$\begin{aligned} b_p(k,\mathbf{r}) &= \sum_{m=-\infty}^{\infty} \exp(\mathrm{i}2\pi mk)\chi_p(\mathbf{r}-\mathbf{A}_p-ma_0\mathbf{e}_z) \\ &= \sum_{m=-\infty}^{\infty} \exp(\mathrm{i}2\pi mk)\chi^m_p(\mathbf{r}) \ , \end{aligned} \tag{3}$$

where p and the vector $\mathbf{A}_p$ represent the label and the position of the atomic function, χ_p, in the reference unit cell, respectively.

The charge neutrality condition of the chain is given by

$$\int_{BZ} dk \sum_n \theta_n(k) = n_e \tag{4}$$

with n_e the number of electrons in the unit cell, and the occupation function $\theta_n(k)$ defined as

$$\theta_n(k) = \begin{cases} 2 & \text{if } E_n(k)\le E_F \\ 0 & \text{if } E_n(k) > E_F \ . \end{cases}$$

The energy bands $E_n(k)$ are the eigenvalues of the RHF equations for Bloch states

$$\begin{aligned} &F(\mathbf{r}_1)\phi_n(k,\mathbf{r}_1) \\ &= \left[-\frac{\nabla^2(\mathbf{r}_1)}{2} - \sum_{m=-\infty}^{\infty}\sum_{a=1}^{M} \frac{Z_a}{|\mathbf{r}_1-\mathbf{A}_a-ma_0\mathbf{e}_z|} \right. \\ &\quad \left. + \int_{BZ} dk' \sum_{n'} \theta_{n'}(k') \int d\mathbf{r}_2 \frac{\phi^*_{n'}(k',\mathbf{r}_2)\phi_{n'}(k',\mathbf{r}_2)}{|\mathbf{r}_1-\mathbf{r}_2|} \right] \\ &\quad \times \phi_n(k,\mathbf{r}_1) \\ &\quad - \frac{1}{2}\int_{BZ} dk' \sum_{n'} \theta_{n'}(k') \int d\mathbf{r}_2 \frac{\phi^*_{n'}(k',\mathbf{r}_2)\phi_n(k,\mathbf{r}_2)}{|\mathbf{r}_1-\mathbf{r}_2|} \\ &\quad \times \phi'_n(k',\mathbf{r}_1) \\ &= E_n(k)\phi_n(k,\mathbf{r}_1) \ , \end{aligned}$$

where $F(\mathbf{r}_1)$ is the Fock operator in the restricted form for double occupancy of the Bloch states, Z_a and the vector $\mathbf{A}_a$ define the nuclear charge and the position of atom a, respectively, and M is the number of atoms. Equation (6) can be cast in matrix form

$$\sum_q F_{pq}(k)C_{qn}(k) = E_n(k)\sum_q S_{pq}(k)C_{qn}(k) \ , \tag{6}$$

where $F_{pq}(k)$ and $S_{pq}(k)$ are the elements of the LCAO Fock $\mathbf{F}(k)$ and overlap $\mathbf{S}(k)$ matrices, defined as

$$F_{pq}(k) = N^{-1}\int d\mathbf{r}b^*_p(k,\mathbf{r})F(\mathbf{r})b_q(k,\mathbf{r}) \tag{7}$$

and

$$S_{pq}(k) = N^{-1}\int d\mathbf{r}b^*_p(k,\mathbf{r})b_q(k,\mathbf{r}) \ . \tag{8}$$

The Fock matrix elements can be written as a sum of three terms

$$F_{pq}(k) = T_{pq}(k) + V_{pq}(k) + X_{pq}(k) \ . \tag{9}$$

$T_{pq}(k)$ is the kinetic energy, $V_{pq}(k)$ the classical electrostatic energy which includes the electron-nuclear attraction and the electron-electron repulsion contributions, and $X_{pq}(k)$ the exchange energy. The analysis of the problems associated with these terms with respect to the convergence of the lattice sums which enter in their definition, the analytic properties of the LCAO density matrix elements $P_{pq}(k)$

$$P_{pq}(k) = \sum_n C^*_{pn}(k)C_{qn}(k)\theta_n(k) \tag{10}$$

in the BZ and the consequences on the RHF results have been documented [31–33].

2.2 Model systems

Depending on the conditions of synthesis and the applied mechanical treatment, POM can exhibit two crystalline structures [34, 35], each corresponding to a different conformation. The most stable form is a structure of hexagonal symmetry [34], in which the chains adopt a 9/5 helical conformation [36]. This conformation corresponds to a C—O—C—O dihedral angle of 78°. In the orthorhombic-symmetry structure [35, 37], which is unstable at room temperature and pressure [38], POM chains have a 2/1 helical structure with a C—O—C—O dihedral angle of 63.7°.

In order to describe specific interactions between hydrogen atoms or between lone pairs, we consider two conformations of the POM chains: a hypothetical zigzag planar (PZZ) form and a 2/1 helical (gauche) form denoted G. The PZZ conformer corresponds to a C—O—C—O dihedral angle (τ) of 180°, and the G conformer to $\tau = 60°$. For both the PZZ and G conformations, tetrahedral angles have been assumed between the C—O—C, O—C—O, H—C—O and H—C—H bonds, and the C—H and C—O distances have been set equal to 1.1066 Å and 1.4306 Å, respectively. These two unit cell geometries are illustrated in Fig. 1.

The band structures obtained for the PZZ and G POM chains are compared with those of a PZZ and hypothetical G chain of PE (Fig. 2). For PE in PZZ and G conformations, standard bond distances have been used (1.54 Å and 1.08 Å for C—C and C—H, respectively) and tetrahedral angles have been assumed for C—C—C, C—C—H and H—C—H.

2.3 Computational aspects

The FSGO band structure calculations are carried out within the Fourier space (FS) RHF approach using a new computational technique designed to evaluate rapidly all lattice summations to convergence [20]. It is beyond the scope of this paper to give a thorough account of the procedure. It is sufficient to say that both the Coulomb and the exchange lattice summations are accurately computed thanks to a combination of the Ewald technique [39] and the Poisson formula [40], the latter being applicable due to expansion of the atomic orbitals in terms of Gaussian functions.

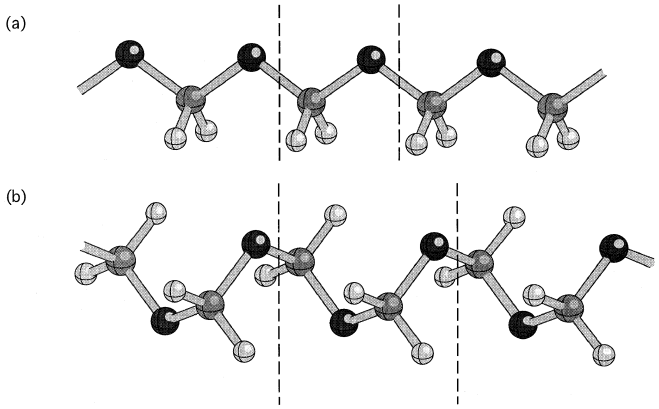

Fig. 1a, b. Geometries of the **a** zigzag planar (PZZ) and **b** gauche (G) conformations of the polyoxymethylene (POM) chains. The unit cell boundaries are denoted by *dotted lines*

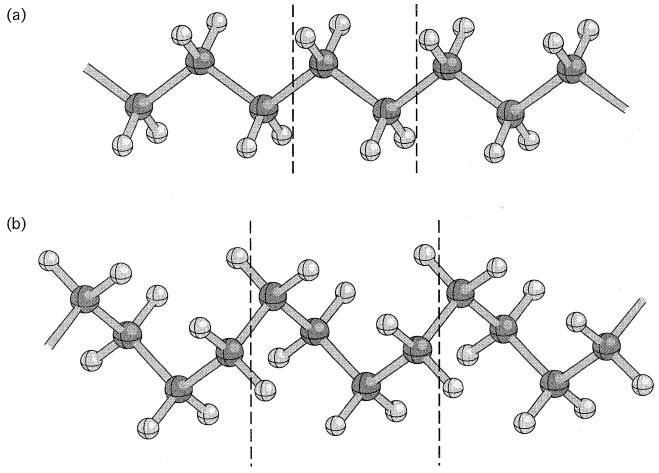

Fig. 2a, b. Geometries of the **a** PZZ and **b** G conformations of the polyethylene (PE) chains. The unit cell boundaries are denoted by *dotted lines*

FSGOs correspond to *s*-type Gaussian orbitals which are allowed to float in space so as to optimally represent each localized pair of electrons. They are defined as

$$g_i(\mathbf{r}) = \left(\frac{2\alpha_i}{\pi}\right)^{3/4} \exp\left(-\alpha_i(\mathbf{r} - \mathbf{R}_i)^2\right) \tag{11}$$

where both the position $\mathbf{R}_i$ and the orbital exponent α_i are used as variational parameters. The FSGO basis set is often referred to as subminimal, since only one function is required to represent an electron pair. The number of basis functions matching the number of electron pairs, the density matrix, is uniquely defined as the inverse of the overlap matrix and the iterative SCF procedure is thus avoided.

Few optimized exponents and positions of FSGOs for extended systems are available in the literature. For the PE translational unit cell, the FSGO basis set consists of two core C_{1s}, two C—C bond and four C—H bond orbitals. In this case, orbital exponents and positions are taken from the literature [17]. The exponents and positions of the FSGOs that we have used for the PE chains are listed in Table 1. For the POM chain, the FSGO basis set consists of one core C_{1s}, one core O_{1s}, two C—O bond, two C—H bond and two O lone-pair (O-LP) orbitals. We have not been able to find the corresponding optimized exponents and positions of the FSGOs for POM in the literature. The parameters for the C_{1s}, O_{1s} and C—H bond orbitals used correspond to those optimized for the CH_4 and H_2O molecules [14]. The C—O bond exponent and position with respect to displacement along the bond axis have been optimized by minimizing the total energy of dimethyl-ether using the GAMESS program [41]. We have also attempted to optimize the exponent of the O-LP orbitals and the LP-O-LP angle. It is not possible to fully optimize the position of the O-LP orbitals without collapse of the orbitals into the O nucleus. Thus, we have arbitrarily chosen to use the O-LP distance given in Ref. [14] for H_2O. We have checked that the small changes in the exponents and positions of the FSGOs resulting from optimization have very little influence on the band structures of the POM chain. The exponents and positions of the FSGOs used for the POM chains are listed in Table 2.

The FSGO band structures obtained by the FS approach have been checked against ab initio band structure calculations in a conventional DS approach using the PLH-93 program [42]. The FS and DS results are in perfect agreement. The STO-3G calculations have been carried out within the DS approach.

Table 1. Exponents and positions (distance from the heavy atom) of the floating spherical gaussian orbitals (FSGOs) for the polyethylene (PE) chains

Basis function	Exponent	Distance from the heavy atom (Å)
C_{1s}	9.306408	0.0
C—H	0.345046	0.6473
C—C	0.362941	0.7700

3 Results and discussion

In this section, we first assess qualitatively the performance of FSGO basis sets in the identification of conformational signatures in the valence band of PE. We then investigate the potential of FSGOs in the description of the long-range interactions in POM which combine both methylenic and oxygen lone pairs cooperative interactions.

3.1 PE chains

In order to study the performance of FSGO basis sets in the description of interactions between hydrogen atoms (hyperconjugation) in polymer chains, we compare the valence-band structures and the valence-band density of states (DOS) of PE in PZZ and G forms obtained using the FSGO and STO-3G basis sets. Previous studies have shown that the STO-3G basis set is sufficient to reproduce the conformational signatures of PE [4] and polypropylene [43]. The total energy E_T, per $-CH_2-CH_2-$ unit, and valence-band energies at selected k-points for the PZZ and G conformations of PE chains using FSGO and STO-3G basis sets are listed in Table 3. The FSGO and STO-3G valence-band structures and valence-band DOS of PE in its two conformations are plotted in Fig. 3.

Comparison of the STO-3G total energies calculated for the two forms of PE shows that the PZZ conformer is more stable by 9.26×10^{-3} a.u. (24.3 kJ mol^{-1}) than the G conformer. As can also be observed from Table 3, the FSGO relative stabilization energy of the PZZ form with respect to the G form is equal to 9.28×10^{-3} a.u. (24.4 kJ mol^{-1}). Thus, the FSGO calculations give the same order for stability and very similar relative energies for PE in its PZZ and G forms as the STO-3G calculations.

The graphs of the FSGO valence-band DOS of PE (Fig. 3a, c; right-hand side) show a marked difference in the relative intensities of the two peaks in the inner-valence region for the PZZ and G conformers. The intensity ratio of the inner-valence peak II, relative to peak I is significantly higher for the PZZ conformer than in the case of the G conformer. The FSGO energy bands (Fig. 3a, c; left-hand side and Table 3) contributing to peak II in the G conformer are characterized by a larger dispersion than in the PZZ chain, 0.21902 and 0.12770 a.u., respectively, while the energy interval corresponding to peak I remains essentially unaffected by the conformation (0.21902 and 0.22384 a.u. for the G and PZZ forms, respectively). The net result is an increase in the intensity of peak II relative to peak I in the case of the PZZ chain compared to the G conformer. Comparison of the energy values listed in Table 3 and the valence-band structures and DOS plotted in Fig. 3 shows that the FSGO and STO-3G results are in good qualitative agreement.

This characteristic sharpening of peak II, which fingerprints the PZZ conformation, is due to the stabilization of band 2 towards the point $k = 0$ (Fig. 3a, b). The FSGO and STO-3G crystalline orbitals belonging to band 2 at $k = 0$ are plotted in Figs. 4a and b, respectively. The shape of the FSGO and STO-3G crystalline orbitals illustrates the nature of the long-range stabilizing interactions, which are through-space interactions of hyperconjugation character between successive CH_2 groups oriented in parallel direction. To understand the origin of the stabilization of the uppermost part of the inner-valence band, it is useful to analyse the composition of the crystalline orbitals at $k = 0$ for the bands 1 and 2, schematically represented in Fig. 5. The FSGOs contributing most to bands 1 and 2 at $k = 0$ (Fig. 5a) are the C—C and C—H, and C—H bond orbitals, respectively. In the case of the STO-3G basis set (Fig. 5b), the inner-valence band switches from a C_{2s} structure to a more stable nodal structure, rich in H_{1s} and C_{2px} orbitals oriented in the direction of the C—H chemical bonds. This mixing of states enables the development of long-range stabilizing interactions between successive methylene groups. The methylenic hyperconjugation along the PE chain in its G form is disfavoured by the rotation of the methylene groups around the C—C bonds from an anti- to a G orientation. Thus, the FSGO basis succeeds in describing specific cooperative hyperconjugation interactions.

Table 3. The total energy E_T, per CH_2-CH_2 unit, and inner-valence band energies at selected k-points, $E_n(k)$ (n being the band index), for the zigzag planar (PZZ) and gauche (G) conformations of PE chains using the FSGO and STO-3G basis sets. Energies are expressed in atomic units

PZZ	FSGO	STO-3G
E_T	66.00446	−77.15871
E_1 (0.0)	−1.01821	−1.06157
E_1 (0.5)	−0.79437	−0.85888
E_2 (0.0)	−0.66667	−0.76447
E_2 (0.5)	−0.79437	−0.85888
G	FSGO	STO-3G
E_T	−65.99518	−77.14945
E_1 (0.0)	−1.03023	−1.08128
$E_{1'}$(0.0)	−0.81072	−0.87751
E_2 (0.0)	−0.81072	−0.87751
$E_{2'}$(0.0)	−0.59170	−0.68044

Table 2. Exponents and positions (distance from the heavier atom) of the FSGOs for the polyoxymethylene (POM) chains. Angle of the lone pair-O-lone pair is equal to 133.5°

Basis function	Exponent	Distance from the heavier atom (Å)
C_{1s}	9.303925	0.0
O_{1s}	17.28454	0.0
C—O	0.503170	0.4787
C—H	0.357486	0.6628
O-lone pair	0.5760	0.2326

3.2 POM chains

The success of the FSGO basis set in the identification of conformational signatures in the valence band of PE has led us to consider POM where oxygen lone pairs replace

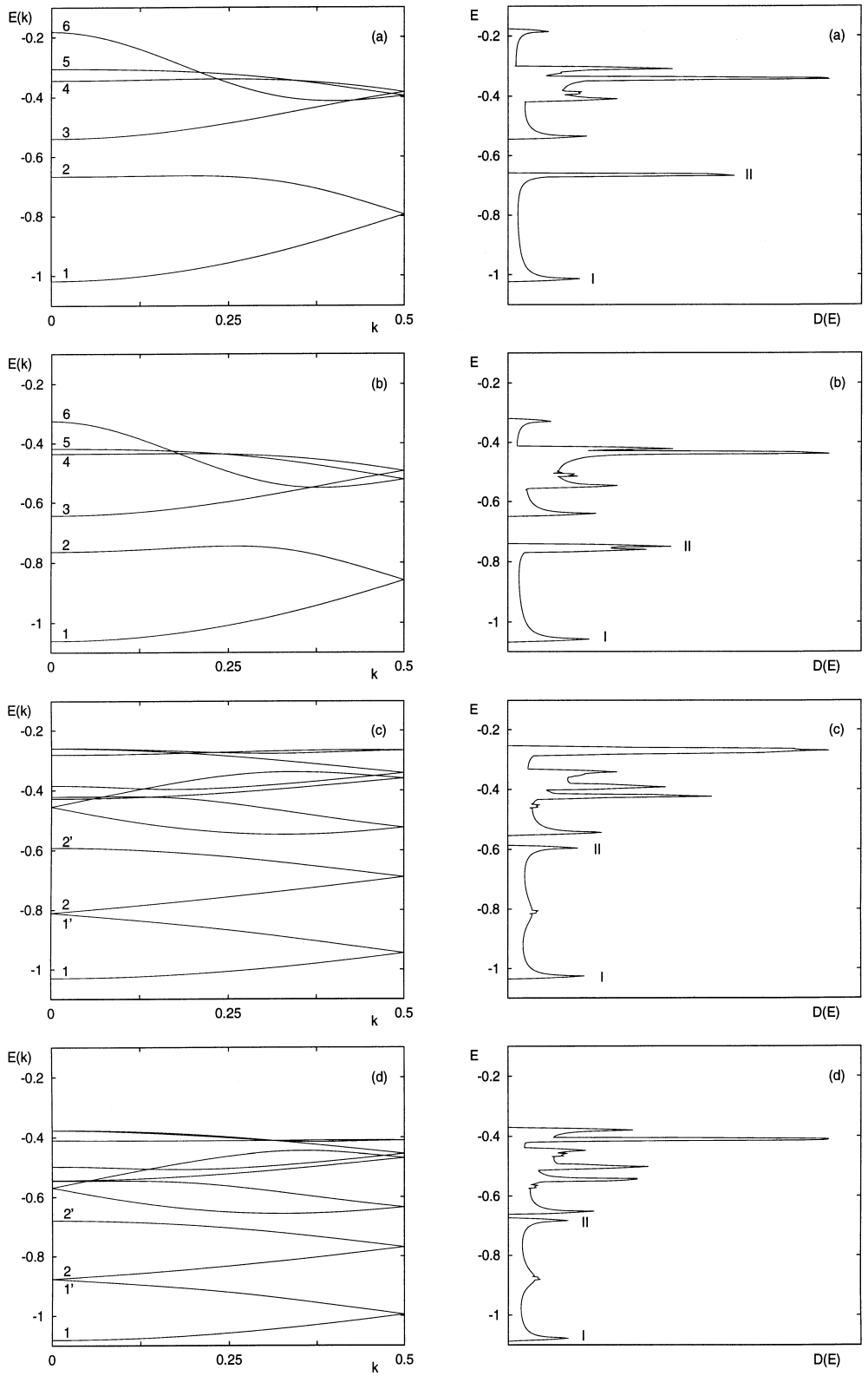

Fig. 3a–d. The valence-band structures (left-hand side) and valence-band density of states (DOS) (right-hand side) of PE in PZZ form obtained using the **a** FSGO basis set, **b** STO-3G basis set, and the G conformer with the **c** FSGO basis set and **d** STO-3G basis set. Energy values are in atomic units and the DOS values are in arbitrary units

hydrogen atoms and could lead to interesting geometry-dependent electronic characteristics. In order to assess the performance of FSGOs in the description of long-range interactions in POM, we compare the valence-band structures and the valence-band DOS of POM in PZZ and G forms obtained using the FSGO and STO-3G basis sets. The total energy E_T, per —CH_2—O— unit, and valence-band energies at selected k-points for the PZZ and G conformations of POM chains using the FSGO and STO-3G basis sets are listed in Table 4.

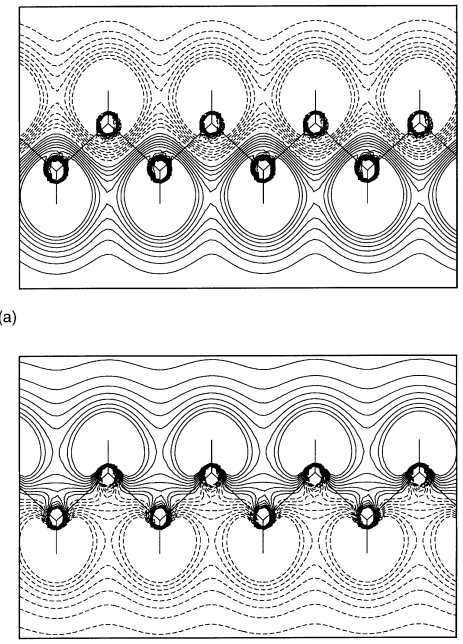

Fig. 4a, b. Shape of the **a** FSGO and **b** STO-3G crystalline orbitals belonging to the uppermost part of the inner-valence region (band 2) at $k = 0$ in the case of the PE chain in PZZ conformation (section along the xz plane defined by the carbon atoms)

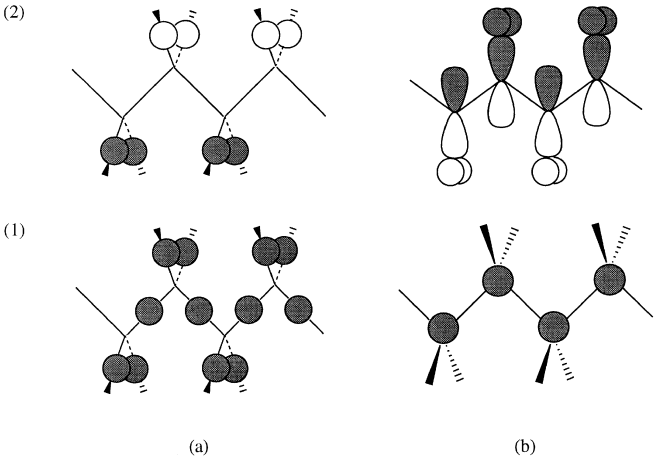

Fig. 5a, b. Sketch of the crystalline orbitals at $k = 0$ in terms of **a** bond orbitals (FSGO basis set) and **b** atomic orbitals (STO-3G basis set) for bands 1 and 2 in the case of the PZZ chain of PE

The FSGO and STO-3G valence-band structures and valence-band DOS of POM in its two conformations are plotted in Fig. 6.

As can be observed from Table 4, the STO-3G relative stabilization energy of the G form with respect to the PZZ form is equal to 5.07×10^{-3} a.u. (13.3 kJ mol^{-1}). This result is in line with previous studies [29, 44]. The FSGO calculations give the same order for stability but predict a much larger energy difference between the PZZ and G forms of POM, 1.62×10^{-2} a.u. (42.5 kJ mol^{-1}), than the STO-3G calculations.

Table 4. The total energy E_T per CH_2—O unit and inner-valence band energies at selected k-points, $E_n(k)$ (n being the band index), for PZZ and G conformations of POM chains using the FSGO and STO-3G basis sets. Energies are expressed in atomic units

PZZ	FSGO	STO-3G
E_T	−96.08581	−112.41214
E_2 (0.0)	−0.76795	−0.84458
E_2 (0.25)	−0.78795	−0.84046
E_2 (0.5)	−0.86726	−0.94098
G	FSGO	STO-3G
E_T	−96.10204	−112.41721
E_2 (0.0)	−0.85754	−0.94343
E_2(0.5)	−0.78327	−0.86015
$E_{2'}$(0.0)	−0.68347	−0.75462
$E_{2'}$(0.5)	−0.78327	−0.86015

Comparison of the inner-valence band structures and DOS of POM plotted in Fig. 6 shows that the FSGO and STO-3G results are in good agreement qualitatively. As can be seen from the graphs of the FSGO valence-band structures and DOS of POM in its two conformations (Fig. 6a, c), the upper part of the inner-valence region exhibits important conformational signatures such as the width of band 2 or the relative intensities of the two bordering peaks, I and II. The intensity ratio of the inner-valence peak II, relative to peak I is significantly higher for the PZZ conformer than in the case of the G conformer. The distribution of states at the bottom of band 2 remains essentially unaffected by the conformation. Indeed, the FSGO energy interval corresponding to peak I is equal to 0.07931 and 0.07427 a.u. for the PZZ and G forms, respectively. On the contrary, the band energies contributing to peak II in the G conformer are characterized by a larger dispersion than in the PZZ chain, 0.09980 and 0.02000 a.u., respectively. The net result is an increase in the intensity of peak II relative to that of peak I in the case of the PZZ chain compared to the G conformer. Comparison of the energy values listed in Table 4 and of the inner-valence band structures and DOS plotted in Fig. 6 shows that the FSGO and STO-3G results compare very well.

As in the case of a PZZ chain of PE, the characteristic sharpening of peak II is due to the stabilization of band 2 towards the point $k = 0$ (Fig. 6a, b). The composition of the crystalline orbitals at $k = 0$ for the bands 1 and 2 are represented schematically in Fig. 7. In the case of the FSGO basis set (Fig. 7a), the inner-valence band switches from a C—O to a C—H and O-lone pair (O-LP) character. Similarly, for the STO-3G basis set (Fig. 7b), there is a switching of the crystalline orbitals at the top of the C_{2s}—O_{2s} band to another nodal structure enriched in H_{1s} atomic functions and C_{2p_x} and O_{2p_x} atomic functions oriented perpendicularly to the direction of periodicity (z-axis). This mixing of states enables the development of long-range stabilizing interactions between successive methylene groups (hyperconjugation) and between lone pairs oriented in parallel directions. The FSGO and STO-3G crystalline orbitals corresponding to band 2 at $k = 0$ are plotted in Fig. 8a, b, respectively. The shape of the crystalline orbitals illus-

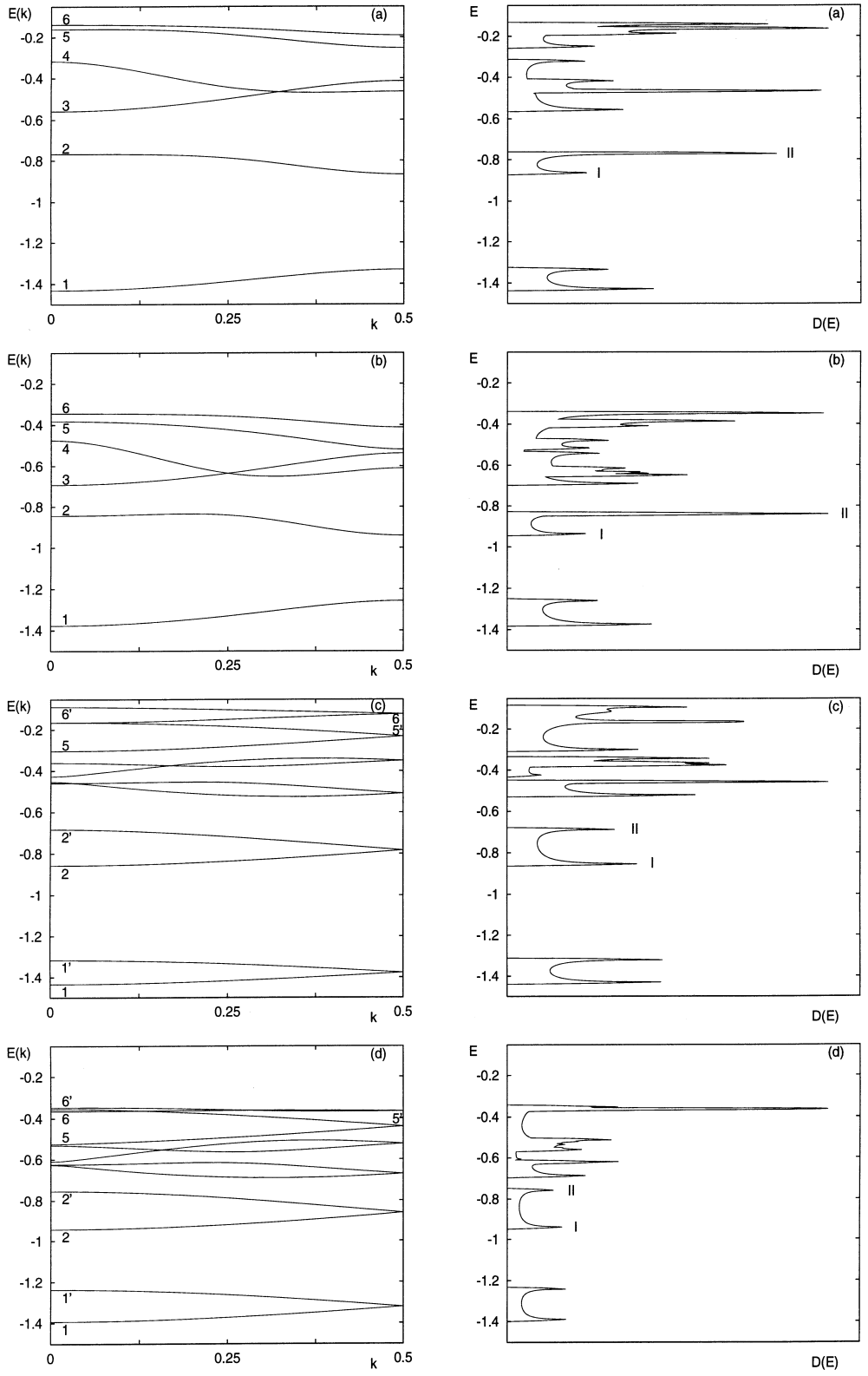

Fig. 6a–d. The valence-band structures (left-hand side) and valence-band DOS (right-hand side) of POM in PZZ form obtained using the **a** FSGO basis set, **b** STO-3G basis set, and the G conformer with the **c** FSGO basis set and **d** STO-3G basis set. Energy values are in atomic units and the DOS values are in arbitrary units

trates the nature of the long-range stabilizing interactions.

In the G structure, the stabilizing interactions along the POM chain are disfavoured by the relative orientation of the C—H and O-LP bond orbitals. The result is a more homogeneous distribution of states at the top of the inner-valence band (band 2′; Fig. 6c, d) and, thus, the widening of peak II.

The graphs of the outer-valence region obtained using the FSGO and STO-3G basis sets show differences such as the width of band 5 in the PZZ conformer (Fig. 6a, b; left-hand side) and of bands 6 and 6′ in the G

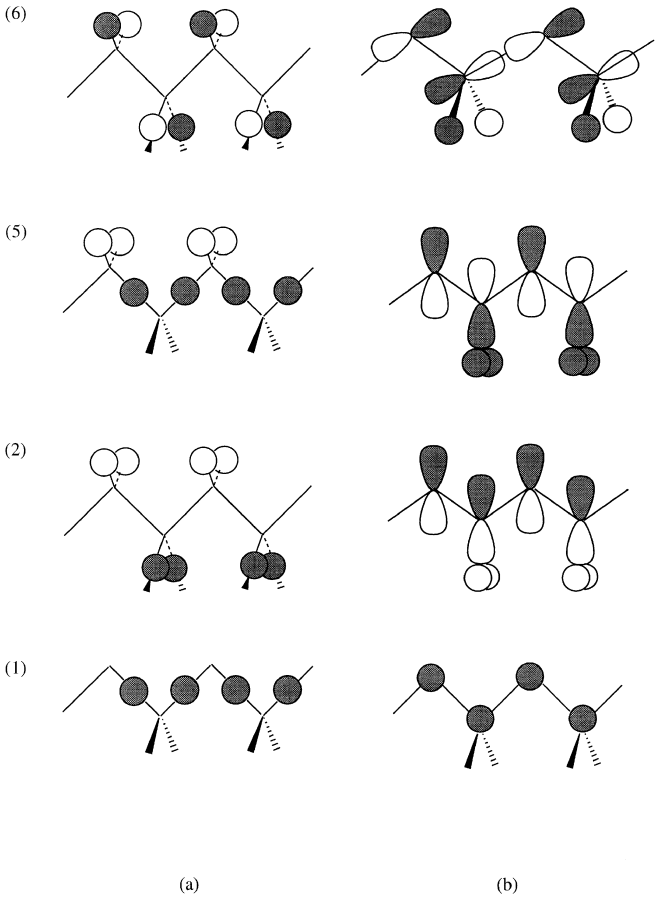

Fig. 7a, b. Sketch of the crystalline orbitals at $k = 0$ in terms of **a** bond orbitals (FSGO basis set) and **b** atomic orbitals (STO-3G basis set) for bands 1, 2, 5 and 6 in the case of the PZZ chain of POM

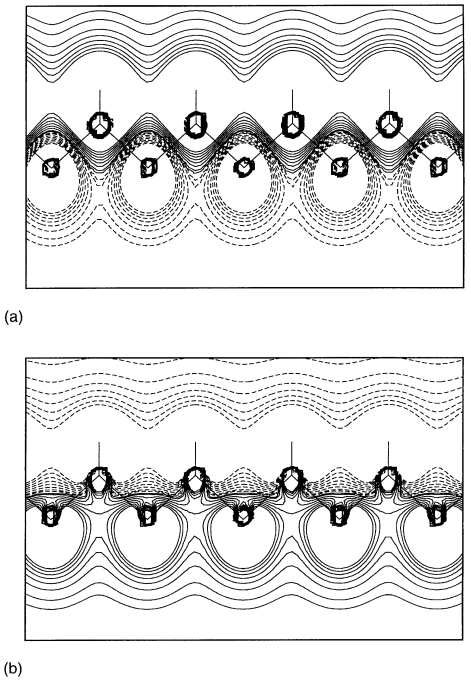

Fig. 8a, b. Shape of the **a** FSGO and **b** STO-3G crystalline orbitals belonging to the uppermost part of the inner-valence region (band 2) at $k = 0$ in the case of the POM chain in PZZ conformation (section along the *xz* plane defined by the carbon and oxygen atoms)

Table 5. Outer-valence band energies at selected *k*-points, $E_n(k)$ (*n* being the band index), for the PZZ and G conformations of POM chains using the FSGO and STO-3G basis sets. Energies are expressed in atomic units

PZZ	FSGO	STO-3G
E_5 (0.0)	−0.16132	−0.38238
E_5 (0.5)	−0.25331	−0.51917
E_6 (0.0)	−0.13846	−0.34417
E_6 (0.5)	−0.19089	−0.41233
G	FSGO	STO-3G
E_5 (0.0)	−0.30394	−0.52504
$E_{5'}$(0.0)	−0.16312	−0.35427
E_6(0.0)	−0.16401	−0.36450
$E_{6'}$(0.0)	−0.08719	−0.34710

conformer (Fig. 6c, d; left-hand side). FSGO and STO-3G valence-band energies at selected *k*-points for the PZZ and G conformations of POM chains are listed in Table 5. As can be seen from Table 5, while the FSGO and STO-3G calculated widths of band 6 (Fig. 6a, b; left-hand side) are comparable (0.05243 and 0.06816 a.u., respectively), the FSGO and STO-3G widths of the corresponding band in the G conformer (bands 6 and 6′; Fig. 6c, d; left-hand side) are very different (0.07682 and 0.01740 a.u.). On the contrary, for band 5, the discrepancy between the FSGO and STO-3G results is much more pronounced in the case of the PZZ conformer (Fig. 6a, b) than in the case of the G conformer (Fig. 6c, d). Indeed, the width of band 5 in the PZZ form is equal to 0.09199 and 0.13679 a.u. for the FSGO and STO-3G basis sets, respectively, while the FSGO and STO-3G widths of bands 5 and 5′ are more comparable (0.14082 and 0.17077 a.u.).

In the case of the STO-3G basis set, the upper part of the outer-valence region, dominantly of O_{2p} atomic functions in character, exhibits conformational dependencies. The crystalline orbitals corresponding to the more energetic of the two O_{2p} bands in the PZZ chain (band 6, Fig. 6b) result from the composition of the O_{2p_y} and C_{2p_y} atomic functions, oriented perpendicularly to the *xz* plane defined by the oxygen and carbon atoms. The atomic functions contributing most to the less energetic of the bands of O_{2p} character (band 5, Fig. 6b) are the O_{2p} and C_{2p} orbitals, parallel to the *xz* plane, and the O_{2s} and C_{2s} orbitals. In the PZZ form, long-range interactions between the O_{2p_y} atomic functions are at the origin of the dispersion of band 6 towards the point $k = 0.5$ (Fig. 6b). On the other hand, such interactions are limited in the G form, yielding a net reduction in the width of the O_{2p_y} band (bands 6 and 6′, Fig. 6d). In the case of the PZZ form, the strong dispersion of the energy levels at the bottom of band 5 is due to through-space interactions between the O_{2p_x} and C_{2p_x} and between the O_{2p_z} and C_{2p_z}. In comparison with the G form, these interactions are favoured by the relative position of atoms in the PZZ chain. Let us note that the dispersion of

bands 5 and 5′ (Fig. 6d) is due to through-space interactions between the O_{2p_z} and C_{2p_z} which also occur in the G form.

The FSGOs contributing most to bands 5 and 6 are the C—O (and O-LP) and O-LP (and C—H) bond orbitals, respectively (Fig. 7a). Despite the fact that the symmetries of bands 5 and 6 are the same using the FSGO and STO-3G basis sets, the FSGO upper part of the outer-valence region (Fig. 6a, c) does not exhibit such a clear dependence upon conformational effects as that observed using the STO-3G basis set. The FSGO basis set thus does not succeed in describing the interactions between the oxygen lone pairs in the POM chains. The large relative stabilization energy of the G form with respect to the PZZ form calculated with the FSGO basis compared to the STO-3G basis set also illustrates the difficulty for the FSGO basis set to represent correctly the oxygen lone pairs.

4 Concluding remarks

In this contribution, it has been shown that the FSGO basis set succeeds in identifying conformational signatures in the inner-valence band of PE. In the case of the POM chain, despite the fact that the inner-valence band structures and DOS obtained using the FSGO and STO-3G basis sets compare very well, the upper part of the outer-valence region using FSGOs does not exhibit as clear conformational dependencies as those observed using the STO-3G basis set. Furthermore, we have seen that the FSGO calculations predict a larger energy difference between the PZZ and G forms of POM than the STO-3G calculations. These discrepancies between the FSGO and STO-3G results in the case of the POM chain are due to the inability of the FSGO basis set to represent correctly the oxygen lone pairs and the interactions between the lone pairs.

As has been shown by previous studies, we can conclude from this work that the approach based on the use of FSGOs provides a simple and computationally fast scheme of calculation that reproduces correctly the bonding trends in polymeric chains. However, important discrepancies are observed in the band structures obtained using the FSGO and STO-3G basis sets. Moreover, very few optimized exponents and positions of FSGOs for extended systems are available in the literature, and the use of FSGOs for practical applications and quantitative results is not realistic. Indeed, the procedure of optimization of FSGOs exponents and positions is not trivial and has to be done for each case studied. The use of standard basis sets is to be preferred. We should also note the importance of calculations on extended systems which can reveal the limits of a method. Nevertheless, the FSGO approach is useful for verification purposes and has enabled us to test the FS-RHF method and the reliability of the Fourier transform code currently limited to just *s*-type Gaussian functions on more chemically interesting systems.

Acknowledgements. I. Flamant thanks Dr. D.H. Mosley for useful discussions and practical help. The calculations reported have been carried out on the "Namur Scientific Computing Facility", with the financial support of the FNRS-FRFC, the "Loterie National" (9.4553.92), and the FNRS/Belgian Ministry of Science "Action d'impulsion à la recherche fondamentale" (D.4511.93).

References

1. Delhalle J, Deleuze M (1992) J Mol Struct (Theochem) 261: 187
2. Deleuze M, Delhalle J, Pickup BT, Svensson S (1994) J Am Chem Soc 116: 10715
3. Riga J, Delhalle J, Deleuze M, Pireaux JJ, Verbist JJ (1994) Surf Interface Anal 22: 507
4. Deleuze M, Denis JP, Delhalle J, Pickup BT (1993) J Phys Chem 97: 5115
5. Deleuze M, Delhalle J, Pickup BT (1993) Chem Phys 175: 427
6. Duwez AS, Riga J, Ghijsen J, Pireaux JJ, Verbist JJ (1995) J Electron Spectrosc Relat Phenom 76: 523
7. Duwez AS, Riga J, Han BY, Delhalle J (1996) J Electron Spectrosc Relat Phenom 81: 55
8. Duwez AS, Di Paolo S, Ghijsen J, Riga J, Deleuze M, Delhalle J (1997) J Phys Chem B 101: 885
9. Frost AA (1967) J Chem Phys 47: 3707
10. Frost AA (1967) J Chem Phys 47: 3714
11. Frost AA (1968) J Phys Chem 72: 1289
12. Christoffersen RE (1971) J Am Chem Soc 93: 4104
13. Cheney BV, Christoffersen RE (1972) J Chem Phys 56: 3503
14. Christoffersen RE, Spangler D, Hall GG, Maggiora GM (1973) J Am Chem Soc 95: 8526
15. André JM, Delhalle J, Demanet C, Lambert-Gérard ME (1976) Int J Quantum Chem Symp 10: 99
16. André JM, Brédas JL (1977) Chem Phys 20: 367
17. André JM, Fripiat JG, Demanet C, Brédas JL, Delhalle J (1978) Int J Quantum Chem Symp 12: 233
18. Delhalle J, André JM, Demanet C, Brédas JL (1978) Chem Phys Lett 54: 186
19. Delhalle J, Harris FE (1985) Phys Rev B 31: 6755
20. Delhalle J, Cizek J, Flamant I, Calais JL, Fripiat JG (1994) J Chem Phys 101: 10717
21. Flamant I, Fripiat JG, Delhalle J (1996) Int J Quantum Chem 60: 1487
22. Flamant I, Delhalle J, Fripiat JG (1997) Int J Quantum Chem 63: 709
23. Del Re G, Ladik J, Biczo G (1967) Phys Rev 155: 977
24. André JM, Gouverneur L, Leroy G (1967) Int J Quantum Chem 1: 427
25. Stewart RF (1970) J Chem Phys 52: 431
26. Boulanger P, Lazzaroni R, Verbist JJ, Delhalle J (1986) Chem Phys Lett 129: 275
27. Cain SR (1988) Chem Phys Lett 143: 361
28. Boulanger P, Riga J, Verbist JJ, Delhalle J (1989) Macromolecules 22: 173
29. Deleuze M, Delhalle J, Mosley DH, André JM (1995) Phys Scr 51: 111
30. Delhalle J, Riga J, Denis JP, Deleuze M, Dosière M (1993) Chem Phys Lett 210: 21
31. Monkhorst HJ (1979) Phys Rev B 20: 1504
32. Monkhorst HJ, Kertesz M (1981) Phys Rev B 24: 3025
33. Delhalle J, Calais JL (1986) J Chem Phys 85: 5286
34. Igushi M, Murase L, Watanabe K (1974) Br Polym J 6: 61
35. Igushi M (1983) Polymer 24: 915
36. Takahashi Y, Tadokoro H (1979) J Polym Sci Polym Phys 17: 123
37. Carazzolo G, Mammi M (1963) J Polym Sci A 1: 965
38. Kobayashi M, Morishita H, Shimomura M, Igushi M (1987) Macromolecules 20: 2453
39. Ewald PP (1921) Ann Phys 64: 253
40. Henrici P (1977) Applied and computational complex analysis. Wiley, New York
41. Schmidt MW, Baldridge KK, Boatz JA, Elbert ST, Gordon MS, Jensen JH, Koseki S, Matsunaga N, Nguyen KA, Su SJ,

Windus TL, Dupuis M, Montgomery JA (1993) J Comput Chem 14: 1347
42. André JM, Mosley DH, Champagne B, Delhalle J, Fripiat JG, Brédas JL, Vanderveken DJ, Vercauteren DP (1993) In: Clementi E (ed) Methods and techniques in computational chemistry, Vol B. Cagliari; Fripiat JG, Mosley DH, Champagne B, André JM (1994) PLH93, an ab initio polymer program
43. Flamant I, Mosley DH, Deleuze M, Andre JM, Delhalle J (1994) Int J Quantum Chem Symp 28: 469
44. Uchida T, Kurita Y, Kubo M (1956) J Polym Sci 29: 365